Cellular and Molecular Life Sciences (2023) 80:19
https://doi.org/10.1007/s00018-022-04669-5

ORIGINAL ARTICLE

Functional screening of congenital heart disease risk loci identifies 5 genes essential for heart development in zebrafish

Jianlong Ma[1] · Yayun Gu[2,3] · Juanjuan Liu[2,4] · Jingmei Song[1] · Tao Zhou[2,4] · Min Jiang[2,4] · Yang Wen[2,3] · Xuejiang Guo[2,4] · Zuomin Zhou[2,4] · Jiahao Sha[2,4] · Jianbo He[1] · Zhibin Hu[2,3,5] · Lingfei Luo[1] · Mingxi Liu[6]

Received: 2 July 2022 / Revised: 9 December 2022 / Accepted: 10 December 2022 / Published online: 27 December 2022

Abstract

Congenital heart disease (CHD) is the most common birth defect worldwide and a main cause of perinatal and infant mortality. Our previous genome-wide association study identified 53 SNPs that associated with CHD in the Han Chinese population. Here, we performed functional screening of 27 orthologous genes in zebrafish using injection of antisense morpholino oligos. From this screen, 5 genes were identified as essential for heart development, including *iqgap2*, *ptprt*, *ptpn22*, *tbck* and *maml3*. Presumptive roles of the novel CHD-related genes include heart chamber formation (*iqgap2* and *ptprt*) and atrioventricular canal formation (*ptpn22* and *tbck*). While deficiency of *maml3* led to defective cardiac trabeculation and consequent heart failure in zebrafish embryos. Furthermore, we found that *maml3* mutants showed decreased cardiomyocyte proliferation which caused a reduction in cardiac trabeculae due to inhibition of Notch signaling. Together, our study identifies 5 novel CHD-related genes that are essential for heart development in zebrafish and first demonstrates that *maml3* is required for Notch signaling in vivo.

Keywords Congenital heart malformation · GWAS · *Danio rerio* · Cardiac development · Notch signaling

Introduction

Congenital heart disease (CHD) is the most common birth defect worldwide and a main cause of perinatal and infant mortality which affect 7–9 per 1000 newborns depending on the population, methods of diagnosis, and severity of the disease [1, 2]. Epidemiological and population-based studies suggest that approximately 20–30% of CHD occurs in the context of syndromes that encompass non-cardiac manifestations, such as Holt-Oram syndrome, DiGeorge syndrome and Noonan syndrome, and for many of these, the primary genetic defect has been identified [3, 4]. The remaining cases represent isolated non-syndromic CHD which refers to CHD with only cardiac abnormalities including simple and severe CHD [5]. Most non-syndromic CHD occur sporadically and may be explained by a multifactorial inheritance model, suggesting that malformations result from multiple susceptibility genes with low-penetrance mutations or intermediate-penetrance mutations in combination with adverse environmental factors [6, 7]. In recent years, several genes have been implicated in monogenic forms of non-syndromic CHD, including *TBX5* and *TBX1* [8]. To identify more common genetic variants associated

Jianlong Ma, Yayun Gu, Juanjuan Liu and Jingmei Song contributed equally to this work.

✉ Lingfei Luo
lluo@swu.edu.cn

✉ Mingxi Liu
mingxi.liu@njmu.edu.cn

1 Institute of Developmental Biology and Regenerative Medicine, Southwest University, Chongqing 400715, China

2 State Key Laboratory of Reproductive Medicine, Nanjing Medical University, Nanjing 211100, China

3 Department of Epidemiology and Biostatistics, School of Public Health, Nanjing Medical University, Nanjing 211100, China

4 Department of Histology and Embryology, Nanjing Medical University, Nanjing 211100, China

5 Key Laboratory of Targeted Intervention of Cardiovascular Disease, Collaborative Innovation Center for Cardiovascular Disease Translational Medicine, Nanjing Medical University, Nanjing 211100, China

6 State Key Laboratory of Reproductive Medicine, The Affiliated Taizhou People's Hospital of Nanjing Medical University, Taizhou School of Clinical Medicine, Nanjing Medical University, Nanjing 211100, China

with sporadic non-syndromic CHD in Han Chinese populations, we performed a multistage genome-wide association study (GWAS) previously [9] and identified 53 SNPs that were associated with CHD. We then identified candidate genes located within 200 kb of these SNPs and ascertained their potential function in CHD by a functional screen of orthologous genes in the zebrafish (*Danio rerio*) model. The zebrafish represents a well-studied model organism in biomedical research because of its rapid development, the large number of eggs produced by a single cross, and the ease of genetic manipulation [10–12]. Additionally, the optical clarity of zebrafish embryos allows for real-time in vivo observation of physiological or pathological events that occur during organ development, rendering zebrafish an optimal vertebrate model system for studying cardiovascular development and homeostasis [13, 14]. The zebrafish has a relatively simple cardiac and vascular system, and the molecular mechanisms underlying vessel formation and morphogenesis are very similar to those of higher vertebrates. In particular, the early stages of zebrafish and human heart development exhibit a remarkable degree of anatomical and functional conservation [15, 16].

Here, we used antisense morpholino oligos (MO) designed against small (~25 bp) regions of mRNA to knock down the genes associated with susceptibility loci identified from CHD GWAS during cardiovascular development. After two rounds of functional screening, we identified 5 novel CHD-related genes that were essential for heart development in zebrafish, including *iqgap2*, *ptprt*, *ptpn22*, *tbck*, and *maml3*. Furthermore, we found deficiency of *maml3* led to abnormal heart morphology and heart failure due to inhibition of Notch signaling. Together, our study identified 5 novel CHD-related genes in regulating zebrafish heart development and demonstrated that *maml3* is required for Notch signaling in vivo. In addition, our results indicated that functional analyses in model systems can effectively translate GWAS findings into relevant biological information in an objective and unbiased manner.

Results

Identification of candidate human CHD susceptibility genes and functional screening of orthologous genes in zebrafish

In our previous GWAS screen involving 4225 CHD cases and 5112 non-CHD controls [9], we identified 53 SNPs that were associated with CHD ($P < 1 \times 10^{-4}$). After 2 rounds of validation with 2160 cases and 3866 controls, we found strong evidence of genome-wide significance ($P < 5 \times 10^{-8}$) for CHD susceptibility for 2 SNPs, rs2474937 at 1p12 ($P = 8.44 \times 10^{-10}$) and rs1531070 at 4q31.1 ($P = 4.99 \times 10^{-12}$). The other SNPs did not reach genome-wide significance ($P < 5 \times 10^{-8}$) by multiple validation analysis; however, they may still mark surrounding genes essential for heart development that confer a risk for CHD. Using *Drosophila* as a model, we have previously shown that functional screening of genes surrounding SNPs that did not reach genome-wide significance can effectively identify disease-related genes and thereby control for false negatives in multiple-stage population data from GWAS [17]. Using a similar strategy, we evaluated genomic regions flanking these potential CHD susceptibility loci (Fig. S1). Outcomes from a recent study revealed that the majority (93%) of disease- and trait-associated SNPs identified by GWAS are located within noncoding sequences [18]. Approximately 32% of GWAS SNPs are located in regulatory DNA marked by deoxyribonuclease I hypersensitive sites (DHSs); these regulator regions may affect genes within 100 kb [18]. We therefore included genes within 200 kb of each SNP and classified these as Class I if the respective SNP was located within the gene body and as Class II if the gene represented an adjacent gene located within 200 kb upstream or downstream of the respective SNP. In total, we identified 56 candidate genes in the human genome that were associated with the 53 SNPs (Table S1 in Supporting Information). We next identified the corresponding zebrafish orthologues using the Ensembl and ZFIN databases and only considered genes with at least 20% sequence identity and of homology type 'orthologue-one to one.' We found 28 orthologous zebrafish genes corresponding to an equal number of human genes (Table S1 in Supporting Information). One orthologous zebrafish gene, *tshz2*, which corresponded to three human genes and three candidate SNPs, was excluded from the functional analysis because antisense morpholino oligos (MO) could not be designed. The remaining 27 genes were included in the next functional study (Fig. S1).

In vivo functional analysis in zebrafish identifies genes essential for heart development

To investigate the function of the 27 zebrafish orthologues during heart development, we conducted an in vivo cardiac development screen using a transgenic zebrafish line *Tg(myl7:GFP)* expressing enhanced green fluorescent protein (GFP) under the control of the cardiac myosin light chain 2 promoter [19]. In this strain, GFP is exclusively expressed in cardiomyocytes such that cardiac development and abnormalities can be clearly visualized during embryonic development. After injection of translation-blocking MO designed against the transcripts of each of the candidate genes (Table S2 in Supporting Information) into 1- to 2-cell stage zebrafish embryos, we assessed the viability and cardiac morphology of embryos at 48 h post-fertilization (hpf) (Fig. S2), when key aspects of heart development including

cardiac chamber and atrioventricular canal (AVC) formation and looping are apparent [20]. For the vast majority (26/27) of candidate genes, knockdown was not associated with a reduction in embryo viability below 50%. *Serp2* morphants exhibited malformation of the whole embryo and less than 50% of embryos were viable, suggesting that this gene plays an essential role during development. *Serp2* was therefore excluded as a candidate CHD susceptibility gene (Fig. S2A). Of the remaining 26 morphants, 7 (29.17%) exhibited a cardiac phenotype with a significantly increased rate of cardiac abnormalities in embryos versus controls (Fig. S2B). The 7 novel genes associated with cardiac defects after MO-mediated knockdown were *iqgap2*, *ptprt*, *tbck*, *ptpn22*, *grm4*, *slc24a3*, and *maml3* (Fig. S3). Among them, 82.80% (207/250) of *iqgap2* morphants and 71.40% (200/280) *ptprt* morphants exhibited a smaller ventricle (Fig. S3B, C); knockdown of *tbck, ptpn22* and *grm4* caused an extended AVC and heart looping defects (Fig. S3D–F); these defects were present in 82.31% (228/277), 85.32% (279/327) and 76.77% (195/254), respectively; While 74.31% (188/253) of *slc24a3* morphants and 73.95% (159/215) *maml3* morphants showed heart looping disorders (Fig. S3G, H). In general appearance, *iqgap2* and *maml3* morphants displayed normal morphology except slight pericardial edema in *iqgap2* morphants (Fig. S3B', H'); knockdown of *ptprt* and *ptpn22* exhibited a smaller head, smaller eyes, unabsorbed yolk, and an edematous hindbrain, while *ptpn22* morphants also showed pericardial edema and curved tail (Fig. S3C′, E′); *tbck*, *grm4,* and *slc24a3* morphants had a smaller head, unabsorbed yolk and pericardial edema (Fig. S3D′, F′, G′).

To exclude the possible off-target effects, splice blocking MOs were designed to verify these phenotypes as second round of validation (Table S2 in Supporting Information) and the effectiveness of these MOs in affecting their target transcripts was confirmed by RT-PCR or sequencing (Fig. S4). Embryos injected with splice blocking MOs of *iqgap2*, *ptprt*, *tbck* and *ptpn22* exhibited similar phenotypes to translation-blocking morphants, confirming an important role of these 4 genes in zebrafish heart development (Fig. 1A–E). While, even the splice blocking morphants of *maml3* presented a similar phenotype, the defects of heart looping were relatively slight and these defects were just present in 55.73% (107/192) (Fig. 1F). However, the phenotypes of *slc24a3* and *grm4* splice blocking morphants were not reproducible, thus we excluded them from further analysis. In summary, we identified 5 genes that had important roles in heart development via a medium-throughput genetic screen based on antisense MOs in zebrafish.

Knockdown of *iqgap2* and *ptprt* causes cardiac chamber defects in developing zebrafish embryos

Similar to translation-blocking morphants, 82.69% (215/260) of *iqgap2* splice-blocking morphants exhibited

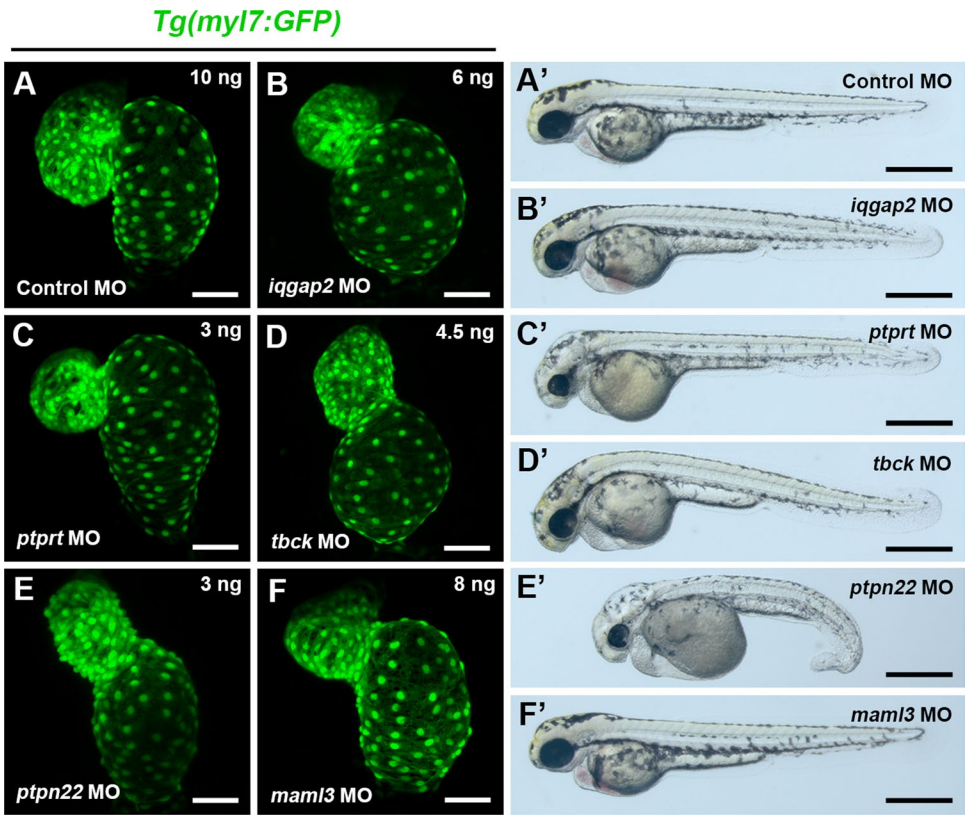

Fig. 1 Cardiac defects induced by knockdown of splice-blocking MO of *iqgap2, ptprt, tbck, ptpn22,* and *maml3*. **A–F** Representative heart images of control and morphant embryos. Ventral view, anterior to the top. Scale bars: 50 μm. **A'–F'** Representative bright-field images of whole embryos. Scale bars: 500 μm

a smaller ventricle and/or an enlarged, balloon-like atrium and mild pericardial edema (Fig. 1B, B'). Double FISH for ventricular and atrial myosin heavy chain (*vmhc* and *amhc*), markers of ventricular and atrial cardiomyocytes, respectively, confirmed this phenotype (Fig. S5A).

Knockdown of *ptprt* with splice-blocking MO was associated with smaller ventricle size, whereas atrium size was not affected. Morphants also had smaller heads and eyes, and an edematous hindbrain (Fig. 1C, C'). These defects were present in 83.56% (244/292) of *ptprt* morphant embryos at 48 hpf. Smaller ventricle size in *ptprt* morphants was also confirmed by double FISH for *vmhc* and *amhc* (Fig. S5A).

The *tbck* and *ptpn22* morphants exhibit an extended AVC and heart looping defects

Consistent with translation-blocking morphants, knockdown of *tbck* and *ptpn22* by splice-blocking MO caused an extended AVC accompanied with heart looping defects (Fig. 1D, E), and these defects were present in 73.33% (209/285), and 73.11% (223/305), respectively. In addition, the *tbck* morphants exhibited smaller head and pericardial edema (Fig. 1D'); And the *ptpn22* morphants had a series of severe morphological defects, including tail curling, hindbrain edema, smaller head, smaller eyes, unabsorbed yolk, and pericardial edema (Fig. 1E'). These results suggest that *tbck* and *ptpn22* play an important role in AVC formation.

To more clearly define the cardiac defects in these two morphants, we examined the expression of the AVC myocardial marker *bmp4* and endocardial marker *has2*. Strikingly, expression of *bmp4* was upregulated and expanded throughout the entire ventricle in both morphants, rather than restricted to AVC region as observed in control MO-injected embryos (Fig. S5B). Similarly, *has2* was also upregulated in these two morphants, with ectopic expression beyond the AVC. However, the cardiac chamber specific markers *vmhc* and *amhc* appeared unaffected in both morphants (Fig. S5B). Overall, we conclude that *tbck* and *ptpn22* do not affect cardiac cell fate specification and patterning, but have an important role in the morphogenesis of the AVC.

To further verify the specificity of the phenotype exhibited in morphants, phenotypic rescue experiments were performed. Knockdown of *iqgap2* with *iqgap2* MO alone caused a smaller ventricle phenotype in 71.3% (72/101) of embryos (Fig. S6B); however, this cardiac chamber defects decreased to 32.3% (31/96) when co-injected *iqgap2* MO with full-length zebrafish *iqgap2* mRNA (Fig. S6B′). Similarly, 65.1% (95/146) and 62.4% (103/165) of embryos showed an extended AVC accompanied with heart looping defects in *tbck* and *ptpn22* MO-injected groups, respectively (Fig. S6C, D). In contrast, such defects were corrected in 34.6% (46/133) and 28.7% (29/101) of embryos when co-injected with full-length *tbck* and *ptpn22* mRNA, respectively (Fig. S6C′, D′). However, *ptprt* mRNA was not able to rescue the cardiac chamber defects in *ptprt* morphants. We speculate that this is caused by the fact that the full-length mRNA of *ptprt* is incomplete in the current database. Together, mRNA rescue experiments further verify the specificity of the phenotype exhibited in *iqgap2*, *tbck*, and *ptpn22* morphants.

Expression pattern of the 5 CHD-related genes in the zebrafish heart

Based on previously reported data [21] and our whole-mount in situ hybridization (WISH) results, with the exception of *iqgap2*, the other 4 novel CHD susceptibility genes were not expressed clearly in the heart region at 24 hpf and 48 hpf (Fig. S7B, C). Besides, these 4 genes were also not expressed in other tissues that may impact heart development indirectly such as bilateral heart fields at 15-somite (Fig. S7A). We assume the expression of these genes was too low to be detected by WISH, and we used the highly sensitive absolute quantitative PCR to measure the absolute copy number of these 5 CHD-related genes in heart tissue. Besides, we also measure the absolute copy number of *myl7*, *ctsk*, and *cryaa* which should have robust, low and no expression in the heart, respectively. The expression level of *ctsk* was lower than *iqgap2*, but higher than *maml3*, *ptprt*, *tbck*, and *ptpn22* (Fig. 2A). Besides, all the 5 CHD-related genes were expressed much higher than *cryaa*, so we assume they were indeed expressed in the heart and could not be noise.

As for *iqgap2*, although it has been mentioned that weak expression of this gene was observed in zebrafish heart, the precise expression pattern of *iqgap2* is not clear [21]. We next assessed the developmental specific expression of *iqgap2* in zebrafish by WISH and detected a low level of *iqgap2* mRNA in the ventricular region at 36 hpf and 48 hpf (Fig. 2B). FISH-antibody staining confirmed the expression of *iqgap2* in the ventricle at 36 hpf and 48 hpf (Fig. 2C). Together, these data suggest that *iqgap2* is expressed in ventricle during heart development, which strongly implies that *iqgap2* plays a significant role in zebrafish ventricular development.

Regional association plots for 3 novel CHD associated loci

Our experimental strategy combining GWAS data with functional screening identified 5 novel CHD susceptibility genes, *TBCK, PTPN22, IQGAP2, PTPRT,* and *MAML3* as essential for cardiac development. Figure S8A-C shows regional risk association plots for the 3 SNPs in the vicinity of *TBCK, PTPN22,* and *IQGAP2*, respectively. Regional risk

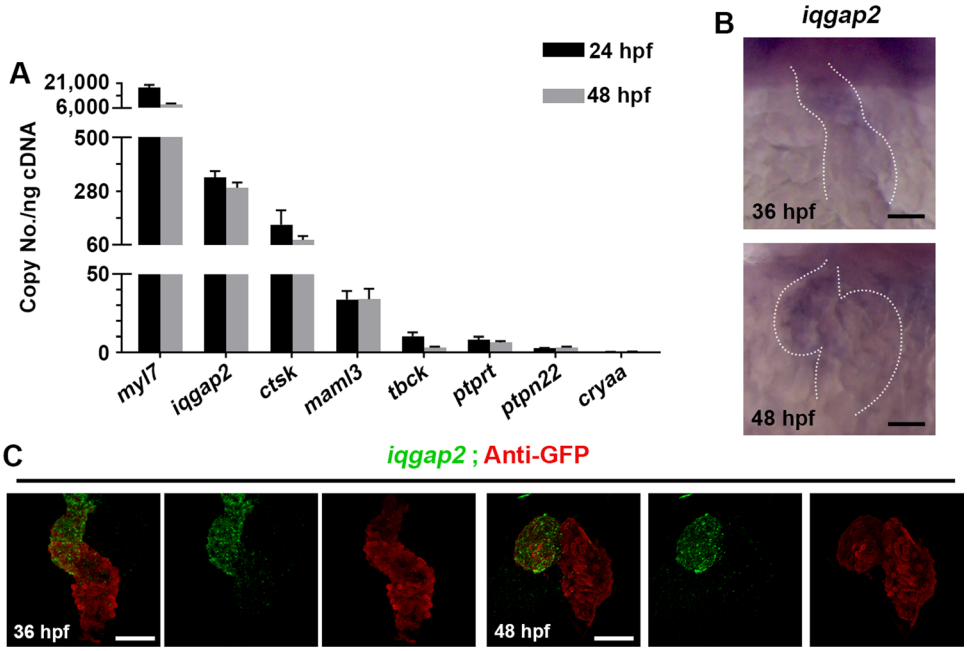

Fig. 2 Expression of *iqgap2, ptprt, tbck*, *ptpn22* and *maml3* in zebrafish heart. **A** Absolute q-PCR analysis of the expression of *myl7*, *ctsk*, *cryaa*, and the 5 CHD-related genes in zebrafish heart at 24 hpf and 48 hpf. Data represent mean ± SEM. **B**. The expression of *iggap2* was assessed in zebrafish embryos at 36 hpf and 48 hpf by WISH. Dotted lines outline the heart. Ventral view, anterior to the top. Scale bars: 50 µm. **C** FISH-antibody staining for *iqgap2* in *Tg(myl7:GFP)* embryos at 36 hpf and 48 hpf

association of rs1531070 with *MAML3* and rs490514 with *PTPRT* has been reported previously [9, 22].

The *maml3*-deficient zebrafish is generated by CRISPR/Cas9 technology

As previously reported, non-syndromic CHD occurs just as a heart defect without other organs anomaly. The *maml3* morphants displayed nearly normal morphology in general appearance (Fig. 1F') that is consistent with non-syndromic CHD. So we generated a *maml3* mutant zebrafish line (*maml3*^{cq131}) using CRISPR/Cas9 technology to further study the biological function of *maml3* in zebrafish heart development (Fig. S9). As indel mutations may not completely disrupt the function of target gene [23], we deleted part of exon 1 and exon 2 of the *maml3* gene by Co-injection of two gRNAs together with Cas9 mRNA (Fig. S9A). PCR amplification of genomic DNA isolated from the microinjected or the wild-type embryos (Fig. S9B) and sequencing of the PCR products (Fig. S9C) indicated the genomic sequence between the two target sites was deleted accurately.

The *maml3* deficiency leads to abnormal heart morphology, impaired cardiac function, and heart failure

To better analyze the heart morphology in *maml3* mutants, we crossed the *maml3*^{cq131} line with the transgenic line *Tg(myl7:GFP)* expressing GFP in cardiomyocytes as mentioned above and the heart defects were analyzed carefully. About 60% of *maml3* mutants presented with slight cardiac looping defects compared with siblings at 2–3 dpf, which is similar to *maml3* morphants (Fig. 3A). While the heart looping defects of *maml3* mutants became apparent at 4–5 dpf (Fig. 3A) and about 15% of *maml3* mutants showed collapsed chambers at 5 dpf (Fig. S10A). In the bright-field view, *maml3* mutant larvae displayed a significant decrease in body length from 3 dpf compared with siblings (Fig. 3B, D). Besides, nearly all the mutant larvae exhibited smaller lens and most mutant larvae have no swim bladder (Fig. 3B). In addition, about half of the *maml3* mutants began to develop pericardial edema at 3 dpf (Fig. 3B), and about 10% of *maml3* mutants showed body edema and decreased blood circulation at 5 dpf (Fig. S10B and Movies S1, S2). Then, we analyzed the heart rate of sibling and *maml3* mutant embryos from 2 to 5 dpf. At 2–4 dpf, heart rate showed no significant difference between sibling and *maml3* mutant larvae (Fig. 3E). While, *maml3* mutants displayed a significantly depressed heart rate at 5 dpf compared with siblings, which indicated that *maml3* mutant larvae developed abnormal cardiac function at 5 dpf (Fig. 3E). In addition, we examined the expression level of *maml3* from 3 to 5 dpf by FISH-antibody staining and found that *maml3* was lowly expressed in heart region at these stages (Fig. 3F). This result implies that *maml3* plays a role in zebrafish heart development from 3 to 5 dpf.

It has been reported that heart failure in zebrafish should include the following components: increased ventricular size, impaired contractility indicated by blood flow, increased edema, cardiac arrhythmias, and increased expression of heart failure biomarkers [24]. As the *maml3* mutants exhibited decreased blood circulation, pericardial edema, and depressed heart rates (Fig. 3 and Fig. S10), we suspect that the mutants developed heart failure. As we

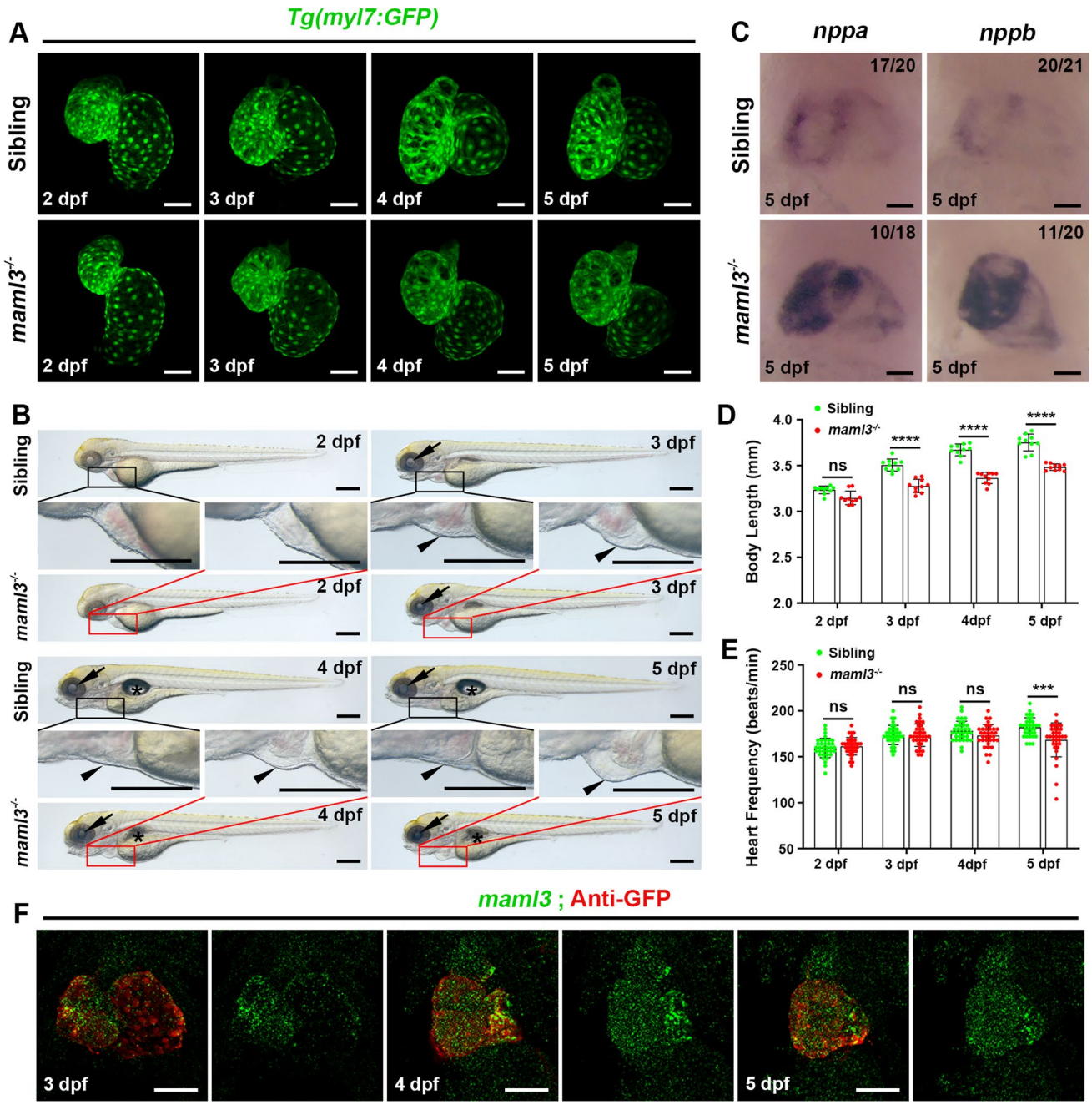

Fig. 3 The *maml3* mutants display abnormal heart morphology, cardiac dysfunction, and heart failure. **A** Representative heart images of siblings and *maml3* mutants from 2 to 5 dpf. Ventral view, anterior to the top. Scale bars: 50 μm. **B** Representative bright-field images of sibling and *maml3* mutant larvae from 2 to 5 dpf. Arrows, arrowheads, and asterisks indicate the lens, pericardium, and swim bladders, respectively. Scale bars: 300 μm. **C** WISH analysis of *nppa* and *nppb* of sibling and *maml3* mutant embryos at 5 dpf. Ventral view, anterior to the top. Scale bars: 50 μm. **D** Mean body length of sibling and *maml3* mutant larvae from 2 to 5 dpf. Data represent mean ± SEM. ns, no significance; $^{****}P < 0.0001$. Student's *t* test. **E** Comparison of the heart rate (beats per minute) in sibling and *maml3* mutant embryos from 2 to 5 dpf. Data represent mean ± SEM. ns, no significance; $^{***}P < 0.001$. Student's *t* test. **F** FISH-antibody staining for *maml3* in *Tg(myl7:GFP)* embryos at 3 dpf, 4dpf, and 5 dpf. Ventral view, anterior to the top. Scale bars: 50 μm

know, natriuretic peptides A and B (*nppa* and *nppb*) are well-known biomarkers of heart failure and are extensively induced in ventricular during heart failure [24–26]. So, we examined the expression of *nppa* and *nppb* and found significantly increased expression of these two markers in the ventricular region of some *maml3* mutants compared with siblings at 5 dpf (Fig. 3C), which further indicated *maml3* mutant embryos develop heart failure. Together,

except normal ventricular size, *maml3* mutants showed all symptoms of heart failure. These data suggested that *maml3* plays an essential role in zebrafish heart development and loss-of-function mutation in *maml3* gene leads to heart failure in zebrafish.

The *maml3* mutants show defective trabeculation

Embryonic heart failure, which is a common cause of morbidity and mortality in CHD, can be induced by abnormal ventricular trabeculation [27–29]. Previous studies showed that a reduction in trabeculation commonly leads to heart failure and early embryonic lethality in both zebrafish and mouse [30, 31]. So we detect whether the trabeculation is perturbed in *maml3* mutants. As cardiac trabeculae are detectable around 3 dpf in zebrafish [30, 32], we observed trabeculation from 3 to 5 dpf in *maml3* mutants. Although a radially arranged protrusion was readily discernible in siblings at 3 dpf, there was less and/or short trabeculae in about 30% of the *maml3* mutants (Fig. 4A, B). In siblings, trabeculae became more pronounced and complex at 4 dpf and formed an elaborate network at 5 dpf (Fig. 4C, E). While about 20% of the *maml3* mutants still showed poorly developed trabeculae carneae at 4–5 dpf (Fig. 4D, F). 3D surface reconstructions of sibling and *maml3* mutant ventricles from 3 to 5 dpf further confirmed the reduced trabecular complexity in *maml3* mutant hearts (Fig. 4A'–F'). Taken together, we assume the phenotype of heart failure in *maml3* mutants is caused by a significant reduction in trabeculation.

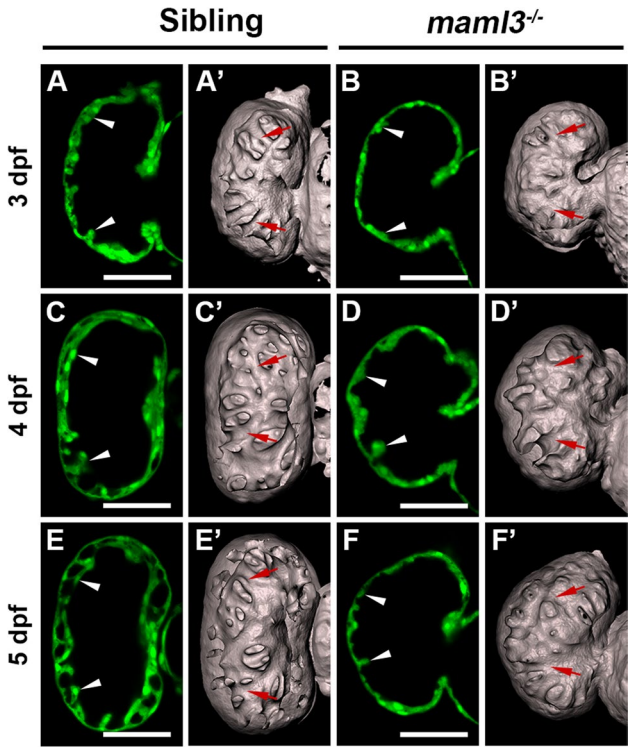

Fig. 4 Knockout of *maml3* leads to a reduction in trabeculae in zebrafish. **A**–**F** Representative ventricle images of siblings (**A**, **C**, **E**) and *maml3* mutants (**B**, **D**, **F**). White arrowheads indicate the trabeculae of siblings and *maml3* mutants. Ventral view, anterior to the top. Scale bars: 50 μm. **A'**–**F'** Surface rendering of the ventricles of siblings (**A'**, **C'**, **E'**) and *maml3* mutants (**B'**, **D'**, **F'**). Red arrows indicate the trabecular ridges of siblings and *maml3* mutants

Notch signaling is down-regulated in *maml3* mutants

To explore the regulatory mechanism of the *maml3* gene involved in zebrafish heart development, we dissected the hearts from siblings or *maml3* mutants at 3 dpf in *Tg(myl7:GFP)* background to perform RNA-Seq analysis. Transcriptional profile analyses revealed down-regulation of Notch signaling related gene in the mutant hearts (Fig. 5A). qPCR verified that the expression of Notch target genes (*hey1*, *hey2,* and *her6*) significantly decreased in the *maml3* mutants (Fig. 5B). These results were surprising, as previous study showed that *Maml3*-null mice exhibited no obvious abnormalities and unchanged mRNA levels of Notch target genes [33]. To further confirm the change of Notch signaling in zebrafish *maml3* mutant, we crossed this mutant line with the Notch reporter line *Tg(Tp1:d2GFP)* expressing a destabilized GFP upon Notch activation [34] and the *Tg(myl7:CFPNTR)*^{cq132} line expressing CFP under the cardiac myosin light chain 2 promoter. Then, Notch activity was assessed in this double transgenic fish at 3 dpf and 5 dpf, respectively. As previously reported [35], Notch-activated *Tp1:*d2GFP was prominent in a subset of ventricular cardiomyocytes and AV endocardial cells at 3 dpf while the *Tp1:*d2GFP^{+} signal gradually declined at 5 dpf in siblings (Fig. 5C, arrows). These *Tp1:*d2GFP^{+} cardiomyocytes in the myocardial wall form clusters across the surface of the ventricle in 3D images (Fig. 5C, arrows). However, *maml3* mutant cardiomyocytes exhibited very weak *Tp1:*d2GFP^{+} signal in the ventricular cardiomyocytes at 3 or 5dpf (Fig. 5C, arrowheads), while the *Tp1:*d2GFP^{+} signal had no significant difference in AV region between siblings and mutants (Fig. 5C, asterisks). These results indicate that *maml3* deficiency leads to a decrease in Notch signaling in the ventricular cardiomyocytes, not the AV region. As Notch activity in the ventricular zone is required for proper trabeculae development [36, 37], we assume trabeculation defect in the *maml3* mutant is caused by decreased Notch signaling.

The *maml3* mutants exhibit decreased cardiomyocyte proliferation

As Notch signaling is essential for regulating cardiomyocyte proliferation during ventricular trabeculation

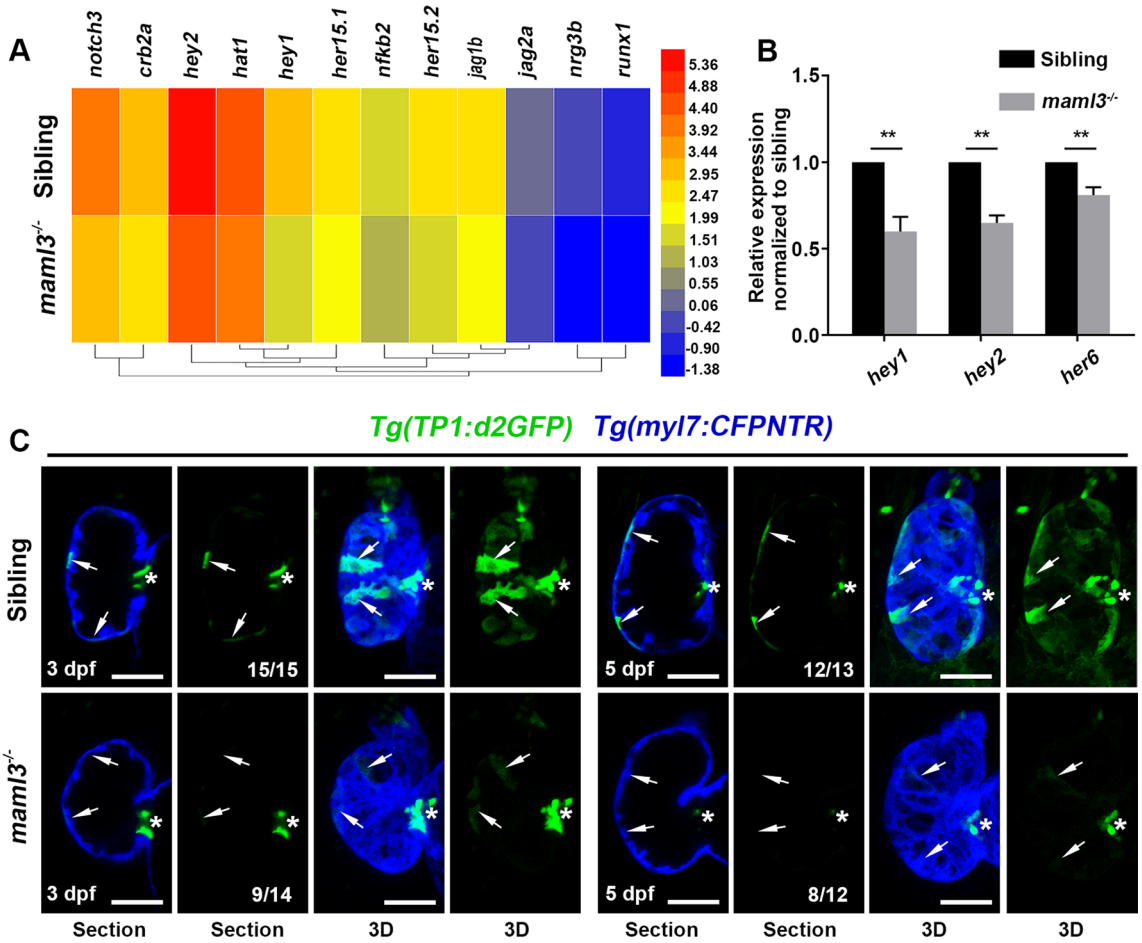

Fig. 5 Notch signaling is down-regulated in *maml3* mutant embryos. **A** Heatmap represents the expression analysis of genes related with Notch signaling pathway in siblings and *maml3* mutant. Bar on the right represents the abundances of expression; color shading from blue to red indicates the expression abundances from low to high. **B** qPCR of representative Notch target genes for cardiac tissue from siblings and *maml3* mutant embryos at 3 dpf. Data represent mean ± SEM. $^{**}P < 0.01$. Student's *t* test. **C** Confocal slices and 3D projections of the ventricles of siblings and *maml3* mutants. Ventral view, anterior to the top. Arrows indicate the *Tp1:*d2GFP^{+} cardiomyocytes and asterisks indicate AV endocardial cells. Ventral view, anterior to the top. Scale bars: 50 μm

in mouse [36], we assumed the reduction in trabeculae in *maml3* mutants caused by decreased ventricular cardiomyocyte proliferation. To assess if cardiomyocyte proliferation was impaired in *maml3* mutants with defective trabeculae, we immunostained for proliferating cell nuclear antigen (PCNA), a marker of cell proliferation and expressed in the nuclei of cells during the DNA synthesis phase of the cell cycle. The *maml3* mutant cardiomyocytes displayed a significantly reduced level of cell proliferation compared with siblings at 3 dpf (Fig. 6A, B), and cardiomyocyte proliferation was further reduced at 4 dpf. In addition, *maml3* mutant larvae also showed a decrease in proliferative ventricular cells using another cell proliferation marker pH3 at 3 dpf(a marker of M phase) (Fig. 6C, D). Similarly, cardiomyocyte proliferation was more significantly suppressed at 4 dpf. These data indicate that the reduced trabeculae in *maml3* mutants is induced by decreased ventricular cardiomyocyte proliferation with inhibition of Notch signaling.

Inhibition of Notch signaling by DAPT in zebrafish shows a similar phenotype to *maml3* mutants

If the cardiac defects in *maml3* mutants were caused by inhibition of Notch signaling, we believed that blocking Notch signaling in wild-type embryos should display a similar phenotype to *maml3* mutants. While, as previously reported, the obvious phenotype of zebrafish embryos treated with high concentrations at 50 μM of DAPT showed a curved tail [38] which does not exhibit in *maml3* mutants. We assumed Notch signaling was just partially inhibited in *maml3* mutants, as the *Tp1:*d2GFP^{+} signal was still present in the AV endocardial cells of *maml3* mutant hearts (Fig. 5C,

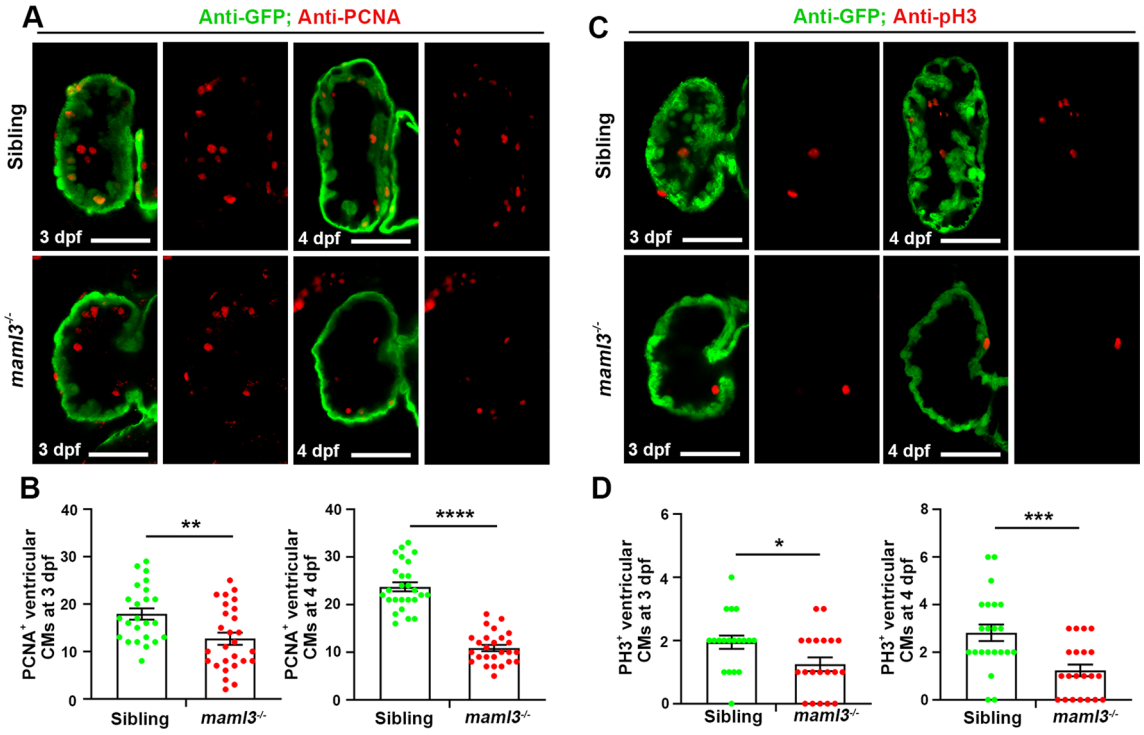

Fig. 6 Reduction in proliferative ventricular cardiac myocytes in *maml3* mutants. **A**, **C** The PCNA and pH3 immunofluorescence staining in *Tg(myl7:GFP)* embryos showed decreased cell proliferative activity in *maml3* cardiomyocytes. Ventral view, anterior to the top. Scale bars: 50 μm. **B**, **D** The number of PCNA and pH3 positive cells in *maml3* mutant ventricles was significantly decreased when compared with siblings. Data represent mean ± SEM. $^{*}P<0.05$; $^{**}P<0.01$***; $P<0.001$; $^{****}P<0.0001$. Student's *t* test

asterisks). To test this hypothesis, we inhibited Notch activity with different concentrations of DAPT starting at 24 hpf and found that most embryos did not show a curved tail when the concentration of DAPT was below 15 μM. So we treated zebrafish embryos with DAPT at 15 μM and observed the cardiac defect when Notch signaling was partially inhibited. The Notch-activated *Tp1:*d2GFP^{+} signals appeared in a subset of ventricular cardiomyocytes and AV endocardial cells in control group at 3 dpf and 5 dpf, whereas these *Tp1:*d2GFP^{+} signals almost disappeared in about half (10/18 in 3 dpf and 8/16 in 5 dpf) of the DAPT-treated embryo hearts (Fig. S11C). Meanwhile, some of DAPT-treated embryos showed similar cardiac defects to *maml3* mutant, including abnormal cardiac looping, defective cardiac trabeculation, and heart failure (Fig. S11A, B). In addition, these embryos displayed pericardial edema and depressed heart rate at 3 and 5 days post-DAPT treatment compared with control group (Fig. S12A, B). Taken together, these data indicate that partial inhibition of Notch signaling with DAPT in zebrafish embryos exhibits a similar phenotype to *maml3* mutant larvae.

Discussion

GWAS was a widely used approach for the identification of susceptibility loci of human disease [39]. However, the biological significance of these SNPs is largely unknown. Considering the highly heterogeneous human population structure and properties of SNPs, many SNPs surrounding causal genes may have been missed due to low association values and multiple validations. To assess the value of SNPs not reaching genome-wide significance, we developed a systematic screening strategy using zebrafish and our previous GWAS data in this study.

Herein, we identified 5 novel CHD-related genes that are essential for embryonic heart development in zebrafish. Previously, we had combined human disease-associated GWAS and animal model screening and identified genes essential for male fertility [17]. We now discovered 5 disease-related genes by selecting genes surrounding SNPs followed by functional screening in zebrafish in the same way. Our approach thus provides a very efficient way to discover risk genes for human disease; moreover, the outcomes of our study suggest GWAS stage data can provide useful information with and without population validation. In addition, different with our previous knockdown strategy on fruit fly of screening for male fertility [17], we perform a second

round validation and 5 MOs were validated in the second round study. Two rounds of knockdown screening help us to discover valid CHD-related genes in a short cycle.

IQGAP2 is a member of the IQGAP family which is relevant to cell migration, cell proliferation, and other cellular processes in humans [40]. There is no report about *IQGAP2* in cardiac development, while deficiency of *IQGAP1*, which is another member of IQGAP family, shows impaired heart function and increased cardiomyocyte apoptosis after pressure overload in mice [41]. Ptprt is a member of the protein tyrosine phosphatase (PTP) family, and interestingly, Ptpn22 is a member of the non-receptor of the PTP family. We found knockdown both of *ptprt* and *ptpn22* exhibited a small head, small eyes, and an edematous hindbrain in zebrafish embryos (Fig. 1C', E'), indicating that these two genes have similar functions. Ptprz, another member of the PTP family, was reported to play essential roles in cardiac development in mouse and zebrafish [42]. While mutation of *PTPN11*, another member of the non-receptor of the PTP family, caused CHD in newborns [43]. Together with our results, we speculated that the PTP family had a close relationship with CHD. Tbck contains a presumptive kinase domain, the TBC (Tre-2/Bub2/Cdc16) domain, and a rhodanese homology domain (RHOD) and is involved in cell proliferation and cell growth [44, 45], which may explain heart abnormalities in *tbck* morphants.

MAML3, a member of Mastermind-like protein family which contain MAML1, MAML2, and MAML3, is a transcriptional coactivator for Notch signaling [46] and there are no reports linking cardiac development with Mastermind-like family to our knowledge. Although *Maml3* is predicted to play an important role in Notch pathway, the majority of research on this gene has been linked to tumors [47–49]. Herein, we found deficiency of *maml3* led to inhibition of Notch signaling and consequent abnormal heart morphology and impaired cardiac function in zebrafish embryos for the first time. While, a previous study showed that *Maml3*-null mice exhibited no decrease in Notch signaling or apparent abnormalities [33]. The discrepancy for the different phenotype in zebrafish and mouse is not fully understood, and it is possible that we deleted partial sequences of *maml3* exon 1 and exon 2 in zebrafish, while only exon 1 of *Maml3* was knocked out in mouse [33]. In addition, although mice are more closely related to humans in evolutionary than zebrafish, for some diseases, the human symptoms can be recapitulated in zebrafish rather than mice. For example, the mutation in human *SEC23B* cause congenital dyserythropoietic anemia type II (CDAII) [50], while deficiency of *Sec23b* in mice has a markedly different phenotype exhibiting abnormalities in pancreas [51]. However, knockdown of zebrafish *sec23b* leads to aberrant erythrocyte development which recapitulates part of the human phenotype [50]. Combined with our previous report which identified the CHD susceptibility loci of rs1531070 at 4q31.1 for *MAML3* in Han Chinese populations [9], we assume the zebrafish *maml3* mutants recapitulate part of the symptoms in CHD patients.

Notch signaling plays important role in cardiac trabeculation, while different components of Notch pathway exhibit diverse functions in different species. For example, deletion of the Notch ligand *Dll4* results in impaired trabeculation in mouse, whereas disruption of another Notch ligand *Jag1* in mouse shows normal cardiac trabeculae [52]. In contrast, zebrafish *jag2b* mutant hearts exhibit increased trabeculation [35]. Herein, we found deficiency of *maml3* led to decrease in ventricular cardiomyocyte proliferation due to inhibition of Notch signaling, which caused impaired cardiac trabeculation and heart failure in zebrafish.

In summary, integrating with our previous GWAS data, we identified 5 novel CHD-related genes that are essential for embryonic cardiac development in zebrafish, including *iqgap2*, *ptprt*, *ptpn22*, *tbck*, and *maml3*. Furthermore, we found that deficiency of *maml3* led to abnormal heart morphology and heart failure due to inhibition of Notch signaling. In addition, our results demonstrate that functional analyses in zebrafish can effectively translate GWAS findings into relevant biological information. The 5 essential risk genes we found warrant further study and may help reveal mechanisms underlying CHD.

Materials and methods

Zebrafish strains

All animal procedures were performed according to protocols approved by the Institutional Animal Care and Use Committee of Southwest University (Approval No. 20140920-01) and were consistent with the National Institutes of Health Guide for the Care and Use of Laboratory Animals. The transgenic or mutant zebrafish lines *Tg(myl7:GFP)* [19], *Tg(Tp1:d2GFP)* [34], *Tg(myl7:CFPNTR)*^{cq132} and *maml3*^{cq131} mutant were used in this study. Embryos were treated with 0.003% 1-phenyl-2-thiourea (PTU, Sigma) from 24 hpf to inhibit pigmentation.

Microinjection of MOs and synthetic mRNAs

MO against each of the 27 candidate genes and a negative control MO was designed by and obtained from Gene tools and injected into 1- to 2-cell embryos to ensure ubiquitous distribution described previously [53–55]. Each of MOs was injected into embryos from a low dose to a high dose (1 ng, 2 ng, 4 ng, 6 ng, 8 ng, and 10 ng per embryo) in MO screen experiment. If embryos exhibited cardiac abnormalities (one or more of the following: developmental delay in AVC

formation, looping defects, a smaller or enlarged atrium or ventricle) when injected with MOs within these doses, we considered these MOs as candidates and established the optimal concentration of each MO according to the embryonic mortality and phenotypic severity in different doses. However, if embryos showed normal hearts even injected with 10 ng MO, we assume that the MO did not affect heart development. MOs used in this study are summarized in Table S2 in Supporting Information. The doses of translation-blocking MOs used in this study are as follows: *iqgap2* MO = 3 ng; *ptprt* MO = 4.5 ng; *tbck* MO = 1.5 ng; *ptpn22* MO = 6 ng; *grm4* MO = 2 ng; *slc24a3* MO = 2 ng; *maml3* MO = 0.8 ng. The doses of splice-blocking MOs used in this study are as follows: *iqgap2* MO = 6 ng; *ptprt* MO = 3 ng; *tbck* MO = 4.5 ng; *ptpn22* MO = 3 ng; *maml3* MO = 8 ng. The viability of zebrafish embryos was ascertained at 48 h post-fertilization (hpf), and morphology was assessed at this time point in all lines with more than 70% viability.

For rescue experiments, full-length cDNAs of *iqgap2*, *ptprt*, *tbck*, and *ptpn22* were subcloned from the pGEMT vector into the pCS2 + vector. Capped mRNA transcripts were generated in vitro from the linearized plasmids using mMESSAGE mMACHINE kit (Ambion) according to the manufacturer's protocol. Each of these mRNAs was co-injected with the corresponding MO at 1- to 2-cell embryos.

Morphology analysis

A total of 200–400 whole embryos were collected in each group, and heart morphology was observed using a fluorescent stereomicroscope (Leica). We graded abnormalities of heart morphology, size and atrioventricular valve as described previously [56–58]. Confocal images were captured by ZEN2010 software equipped on an LSM780 confocal microscope (Carl Zeiss). Bright-field images were captured using a SteREO Discovery V20 microscope equipped with Axio Vision Rel 4.8.2 software (Carl Zeiss).

In situ hybridization and antibody staining

Whole-mount in situ hybridization (WISH), fluorescent in situ hybridization (FISH), and antibody staining were performed as previously described [59–62]. The primers used for probe synthesis are listed in Table S3 in Supporting Information. Images of WISH were captured using a SteREO Discovery V20 microscope equipped with Axio Vision Rel 4.8.2 software (Carl Zeiss). Images of FISH were captured using ZEN2010 software equipped on an LSM780 or LSM880 confocal microscope (Carl Zeiss). Whole-mount antibody staining was performed as previously described [63]. Primary antibodies against PCNA (1:500; Abcam) and pH3 (1:500; Millipore) were applied. Images were captured using ZEN2010 software equipped on an LSM780 or LSM880 confocal microscope (Carl Zeiss).

Dissection of zebrafish heart

Zebrafish heart isolation was performed as previously described [64]. Briefly, zebrafish embryos were anaesthetized (about 800 in number for each sample) in PBS by treatment with tricaine (Sigma, USA). Manually dissect out GFP-positive hearts under a fluorescence stereomicroscope (Leica) with a pair of fine tweezers (WPI) and concentrate them in the center of the dish. Collect the hearts in the smallest possible volume and pipette into a 1.5 ml tube containing 0.75 ml PBS (on ice). Then, the hearts were sedimented by centrifuging at 2,000 × g for 5 min at 4 °C. Carefully remove the supernatant, then add 0.5 ml TriZol (Invitrogen) to the tube containing the sedimented hearts.

Transcriptome sequencing (RNA-Seq)

Three samples each for WT and *maml3* mutant were prepared for sequencing, and mean values were calculated for the final analysis. The RNA library of each sample was constructed and sequenced using an Illumina HiSeq platform by Novogene following their standard procedures. Raw data of fastq format were firstly processed through in-house perl scripts. In this step, clean data were obtained by removing reads containing adapter, reads containing ploy-N and low quality reads from raw data. All the downstream analyses were based on the clean data with high quality. The expressed values of all genes were calculated and normalized to fragments per kilobase of transcript per million mapped fragments (FPKM). FPKM values were obtained from RNA-seq data to generate a heatmap by the Helm software. The color scale shown represents FPKM values which were log2 transformed. Raw data were deposited in the NCBI Sequence Read Archive database under accession number PRJNA900016.

Reverse transcription-polymerase chain reaction (RT-PCR)

To verify the effectiveness of MOs in affecting their target transcripts, RT-PCR was performed. Embryos were injected with MOs at the 1- to 2-cell stage, and total RNA was isolated from whole embryos at 48 hpf using TriZol reagent (Invitrogen). RNA was reverse transcribed into cDNA using OmniScript Reverse Transcription Kit (QIAGEN). The primers used for RT-PCR are listed in Table S3 in Supporting Information.

Absolute quantitative real-time PCR (qPCR)

RT-qPCR was carried out using the FastStart Universal SYBR Green Master (Roche). Total RNA was isolated from heart tissue at 24 hpf and 48 hpf using TriZol reagent (Invitrogen). RNA was reverse transcribed into cDNA using OmniScript Reverse Transcription Kit (QIAGEN). The primers used for RT-qPCR are listed in Table S3 in Supporting Information. For absolute quantification by PCR, *iqgap2*, *ptprt*, *tbck*, *ptpn22*, *maml3*, *myl7* (high expression in heart), *ctsk* (low expression in heart), and *cryaa* (no expression in heart) cDNA fragments were amplified and cloned into pGEMT-Easy vector (Promega) as templates. Each plasmid DNA was tenfold serially diluted from 10^7 to 10^3 copies and used in subsequent experiments for generating standard curve. The qPCR reaction (15 µl) in triplicates comprised of PCR grade water (3.3 µl); SYBR Green (2x, 7.5 µl); Primer F and R (10 pmol/µl, 0.6 µl each) and plasmid DNA(3 µl) or cDNA (10 ng/µl, 3.0 µl). The obtained Ct values were plotted against the logarithm of their template copy numbers of each standard plasmid DNA, and the standard curve was generated by a linear regression of the plotted points. Absolute quantification of the sample of 24hpf and 48hpf was read from the standard curve [65].

Generation of the *maml3*^{cq131} mutant line

The *maml3*^{cq131} mutant line was generated by CRISPR/Cas9 technology as previously described [23]. In brief, two gRNAs (50 pg) together with Cas9 mRNA (300 pg) were co-injected into 1-cell stage wild-type embryos, and the lysate of about 10 embryos at 24 hpf was used as templates for PCR. The PCR products were sequenced to examine the deleted genomic sequences in *maml3* target region, and embryos with effective genome editing were raised to adults (F0). Then, F0 fish were screened to identify the founder whose progeny carry the mutation, and offspring of identified F0 was raised up to get the candidate progeny (F1). Last, individual F1 adults were screened by PCR using the tail fin genomic DNA and the genotypes of mutants were determined by DNA sequencing. The target sequence of *maml3* and PCR primers is depicted in Table S3 in Supporting Information.

Statistical methods

Differences between treatment and control groups after MO injection and assessment at 48 hpf were analyzed using one-way ANOVA and the Fisher's exact test (Stata Software 11.0, Stata Corporation, College Station, TX). Other statistical calculations in this paper were performed using GraphPad Prism 8. Unpaired Student's *t* test was used for statistical analysis. Values of $P < 0.05$ were considered statistically significant (*, $P < 0.05$; **, $P < 0.01$; ***, $P < 0.001$; ****, $P < 0.0001$); ns ($P > 0.05$) indicated not significant. All values were expressed as mean ± SEM.

Supplementary Information The online version contains supplementary material available at https://doi.org/10.1007/s00018-022-04669-5.

Acknowledgements We thank Prof. Peidong Han for providing the *Tg(Tp1:d2GFP)* line.

Author contributions ML, LL, ZH, JS, and ZZ designed the experiments. ML and LL designed the experiments. JM, YG, JL, JS, TZ, MJ, YW, XG, and JH performed most experiments and analysis. ML wrote the manuscript. All authors read and approved the final version of the manuscript.

Funding This work was supported by the National Key Project of Research and Development Program (2018YFC1004200, 2018YFC1004202), the Program of the National Natural Science Foundation of China (81830100), and the National Key R&D Program of China (2021YFA0805000).

Data availability The datasets used and/or analyzed during the current study are available from the corresponding author on reasonable request.

Declarations

Conflict of interest The authors declare that they have no competing interests.

Ethics approval All animal procedures were performed according to protocols approved by the Institutional Animal Care and Use Committee of Southwest University (Approval No. 20140920-01).

Consent to participate This article does not contain any studies involving human participants performed by any of the authors.

References

1. van der Linde D, Konings EE, Slager MA, Witsenburg M, Helbing WA, Takkenberg JJ, Roos-Hesselink JW (2011) Birth prevalence of congenital heart disease worldwide: a systematic review and meta-analysis. J Am Coll Cardiol 58:2241–2247
2. Liu Y, Chen S, Zuhlke L, Black GC, Choy MK, Li N, Keavney BD (2019) Global birth prevalence of congenital heart defects 1970–2017: updated systematic review and meta-analysis of 260 studies. Int J Epidemiol 48:455–463
3. Landis BJ, Cooper DS, Hinton RB (2016) CHD associated with syndromic diagnoses: peri-operative risk factors and early outcomes. Cardiol Young 26:30–52
4. Øyen N, Poulsen G, Boyd HA, Wohlfahrt J, Jensen PKA, Melbye M (2009) Recurrence of congenital heart defects in families. Circulation 120:295–301
5. Yang L, Liu X, Chen Y, Shen B (2021) An update on the CHDGKB for the systematic understanding of risk factors associated with non-syndromic congenital heart disease. Comput Struct Biotechnol J 19:5741–5751

6. Ware S, Jefferies J (2012) New genetic insights into congenital heart disease. J Clin Exp Cardiolog S8:003
7. Yasuhara J, Garg V (2021) Genetics of congenital heart disease: a narrative review of recent advances and clinical implications. Transl Pediatr 10:2366–2386
8. Wessels M, Willems P (2010) Genetic factors in non-syndromic congenital heart malformations. Clin Genet 78:103–123
9. Hu Z, Shi Y, Mo X, Xu J, Zhao B, Lin Y, Yang S, Xu Z, Dai J, Pan S et al (2013) A genome-wide association study identifies two risk loci for congenital heart malformations in Han Chinese populations. Nat Genet 45:818–821
10. Lieschke GJ, Currie PD (2007) Animal models of human disease: zebrafish swim into view. Nat Rev Genet 8:353–367
11. Francoeur N, Sen R (2021) Advances in cardiac development and regeneration using zebrafish as a model system for high-throughput research. J Dev Biol 9:40
12. Brittijn SA, Duivesteijn SJ, Belmamoune M, Bertens LFM, Bitter W, de Bruijn JD, Champagne DL, Cuppen E, Flik G, Vandenbroucke-Grauls CM et al (2009) Zebrafish development and regeneration: new tools for biomedical research. Int J Dev Biol 53:835–850
13. Gays D, Santoro MM (2013) The admiR-able advances in cardiovascular biology through the zebrafish model system. Cell Mol Life Sci CMLS 70:2489–2503
14. Bowley G, Kugler E, Wilkinson R, Lawrie A, van Eeden F, Chico TJA, Evans PC, Noël ES, Serbanovic-Canic J (2021) Zebrafish as a tractable model of human cardiovascular disease. Br J Pharmacol 179:900–917
15. Isogai S, Horiguchi M, Weinstein B (2001) The vascular anatomy of the developing zebrafish: an atlas of embryonic and early larval development. Dev Biol 230:278–301
16. Brown DR, Samsa LA, Qian L, Liu J (2016) Advances in the study of heart development and disease using zebrafish. J Cardiovasc Dev Dis 3:13
17. Yu J, Wu H, Wen Y, Liu Y, Zhou T, Ni B, Lin Y, Dong J, Zhou Z, Hu Z et al (2015) Identification of seven genes essential for male fertility through a genome-wide association study of non-obstructive azoospermia and RNA interference-mediated large-scale functional screening in Drosophila. Hum Mol Genet 24:1493–1503
18. Maurano M, Humbert R, Rynes E, Thurman R, Haugen E, Wang H, Reynolds A, Sandstrom R, Qu H, Brody J et al (2012) Systematic localization of common disease-associated variation in regulatory DNA. Science 337:1190–1195
19. Burns CG, Milan DJ, Grande EJ, Rottbauer W, MacRae CA, Fishman MC (2005) High-throughput assay for small molecules that modulate zebrafish embryonic heart rate. Nat Chem Biol 1:263–264
20. Miura G, Yelon D (2011) A guide to analysis of cardiac phenotypes in the zebrafish embryo. Methods Cell Biol 101:161–180
21. Fang X, Zhang B, Thisse B, Bloom GS, Thisse C (2015) IQGAP3 is essential for cell proliferation and motility during zebrafish embryonic development. Cytoskeleton 72:422–433
22. Lin Y, Guo X, Zhao B, Liu J, Da M, Wen Y, Hu Y, Ni B, Zhang K, Yang S et al (2015) Association analysis identifies new risk loci for congenital heart disease in Chinese populations. Nat Commun 6:8082
23. Xiao A, Wang Z, Hu Y, Wu Y, Luo Z, Yang Z, Zu Y, Li W, Huang P, Tong X et al (2013) Chromosomal deletions and inversions mediated by TALENs and CRISPR/Cas in zebrafish. Nucleic Acids Res 41:e141
24. Narumanchi S, Wang H, Perttunen S, Tikkanen I, Lakkisto P, Paavola J (2021) Zebrafish heart failure models. Front Cell Dev Biol 9:662583
25. Becker JR, Robinson TY, Sachidanandan C, Kelly AE, Coy S, Peterson RT, MacRae CA (2012) In vivo natriuretic peptide reporter assay identifies chemical modifiers of hypertrophic cardiomyopathy signalling. Cardiovasc Res 93:463–470
26. Shi X, Verma S, Yun J, Brand-Arzamendi K, Singh KK, Liu X, Garg A, Quan A, Wen XY (2017) Effect of empagliflozin on cardiac biomarkers in a zebrafish model of heart failure: clues to the EMPA-REG OUTCOME trial? Mol Cell Biochem 433:97–102
27. Sedmera D (2009) Pathways to embryonic heart failure. Am J Physiol Heart Circ Physiol 297:H1578-1579
28. Zhang W, Chen H, Qu X, Chang C-P, Shou W (2013) Molecular mechanism of ventricular trabeculation/compaction and the pathogenesis of the left ventricular noncompaction cardiomyopathy (LVNC). Am J Med Genet C Semin Med Genet 163:144–156
29. Meyer HV, Dawes TJW, Serrani M, Bai W, Tokarczuk P, Cai J, de Marvao A, Henry A, Lumbers RT, Gierten J et al (2020) Genetic and functional insights into the fractal structure of the heart. Nature 584:589–594
30. Liu J, Bressan M, Hassel D, Huisken J, Staudt D, Kikuchi K, Poss KD, Mikawa T, Stainier DY (2010) A dual role for ErbB2 signaling in cardiac trabeculation. Development 137:3867–3875
31. Gassmann M, Casagranda F, Orioli D, Simon H, Lai C, Klein R, Lemke G (1995) Aberrant neural and cardiac development in mice lacking the ErbB4 neuregulin receptor. Nature 378:390–394
32. Peshkovsky C, Totong R, Yelon D (2011) Dependence of cardiac trabeculation on neuregulin signaling and blood flow in zebrafish. Dev Dyn 240:446–456
33. Oyama T, Harigaya K, Sasaki N, Okamura Y, Kokubo H, Saga Y, Hozumi K, Suganami A, Tamura Y, Nagase T et al (2011) Mastermind-like 1 (MamL1) and mastermind-like 3 (MamL3) are essential for Notch signaling in vivo. Development 138:5235–5246
34. Clark BS, Cui S, Miesfeld JB, Klezovitch O, Vasioukhin V, Link BA (2012) Loss of Llgl1 in retinal neuroepithelia reveals links between apical domain size, Notch activity and neurogenesis. Development (Cambridge, England) 139:1599–1610
35. Han P, Bloomekatz J, Ren J, Zhang R, Grinstein JD, Zhao L, Burns CG, Burns CE, Anderson RM, Chi NC (2016) Coordinating cardiomyocyte interactions to direct ventricular chamber morphogenesis. Nature 534:700–704
36. Grego-Bessa J, Luna-Zurita L, del Monte G, Bolos V, Melgar P, Arandilla A, Garratt AN, Zang H, Mukouyama YS, Chen H et al (2007) Notch signaling is essential for ventricular chamber development. Dev Cell 12:415–429
37. Samsa LA, Givens C, Tzima E, Stainier DYR, Qian L, Liu J (2015) Cardiac contraction activates endocardial Notch signaling to modulate chamber maturation in zebrafish. Development 142:4080–4091
38. Yang T, Arslanova D, Gu Y, Augelli-Szafran C, Xia W (2008) Quantification of gamma-secretase modulation differentiates inhibitor compound selectivity between two substrates Notch and amyloid precursor protein. Mol Brain 1:15
39. Visscher PM, Wray NR, Zhang Q, Sklar P, McCarthy MI, Brown MA, Yang J (2017) 10 years of GWAS discovery: biology, function, and translation. Am J Hum Genet 101:5–22
40. Hedman AC, Smith JM, Sacks DB (2015) The biology of IQGAP proteins: beyond the cytoskeleton. EMBO Rep 16:427–446
41. Sbroggio M, Carnevale D, Bertero A, Cifelli G, De Blasio E, Mascio G, Hirsch E, Bahou WF, Turco E, Silengo L et al (2011) IQGAP1 regulates ERK1/2 and AKT signalling in the heart and sustains functional remodelling upon pressure overload. Cardiovasc Res 91:456–464
42. Katraki-Pavlou S, Kastana P, Bousis D, Ntenekou D, Varela A, Davos CH, Nikou S, Papadaki E, Tsigkas G, Athanasiadis E et al (2022) Protein tyrosine phosphatase receptor-zeta1 deletion triggers defective heart morphogenesis in mice and zebrafish. Am J Physiol Heart Circ Physiol 322:H8–H24

43. Sarkozy A, Conti E, Seripa D, Digilio MC, Grifone N, Tandoi C, Fazio VM, Di Ciommo V, Marino B, Pizzuti A et al (2003) Correlation between PTPN11 gene mutations and congenital heart defects in Noonan and LEOPARD syndromes. J Med Genet 40:704–708
44. Liu Y, Yan X, Zhou T (2013) TBCK influences cell proliferation, cell size and mTOR signaling pathway. PLoS ONE 8:e71349
45. Wu J, Lu G (2021) Multiple functions of TBCK protein in neurodevelopment disorders and tumors. Oncol Lett 21:17
46. Kitagawa M (2016) Notch signalling in the nucleus: roles of Mastermind-like (MAML) transcriptional coactivators. J Biochem 159:287–294
47. Alzofon N, Koc K, Panwell K, Pozdeyev N, Marshall CB, Albuja-Cruz M, Raeburn CD, Nathanson KL, Cohen DL, Wierman ME et al (2021) Mastermind like transcriptional coactivator 3 (MAML3) drives neuroendocrine tumor progression. Mol Cancer Res 19:1476–1485
48. Wang X, Bledsoe KL, Graham RP, Asmann YW, Viswanatha DS, Lewis JE, Lewis JT, Chou MM, Yaszemski MJ, Jen J et al (2014) Recurrent PAX3-MAML3 fusion in biphenotypic sinonasal sarcoma. Nat Genet 46:666–668
49. Li J, Li T, Lu Y, Shen G, Guo H, Wu J, Lei C, Du F, Zhou F, Zhao X et al (2017) MiR-2392 suppresses metastasis and epithelial-mesenchymal transition by targeting and in gastric cancer. FASEB J 31:3774–3786
50. Schwarz K, Iolascon A, Verissimo F, Trede NS, Horsley W, Chen W, Paw BH, Hopfner KP, Holzmann K, Russo R et al (2009) Mutations affecting the secretory COPII coat component SEC23B cause congenital dyserythropoietic anemia type II. Nat Genet 41:936–940
51. Tao J, Zhu M, Wang H, Afelik S, Vasievich MP, Chen XW, Zhu G, Jensen J, Ginsburg D, Zhang B (2012) SEC23B is required for the maintenance of murine professional secretory tissues. Proc Natl Acad Sci USA 109:E2001-2009
52. D'Amato G, Luxan G, del Monte-Nieto G, Martinez-Poveda B, Torroja C, Walter W, Bochter MS, Benedito R, Cole S, Martinez F et al (2016) Sequential Notch activation regulates ventricular chamber development. Nat Cell Biol 18:7–20
53. Nasevicius A, Ekker SC (2000) Effective targeted gene 'knockdown' in zebrafish. Nat Genet 26:216–220
54. Lu H, Ma J, Yang Y, Shi W, Luo L (2013) EpCAM is an endoderm-specific Wnt derepressor that licenses hepatic development. Dev Cell 24:543–553
55. Yang Y, Wang H, He J, Shi W, Jiang Z, Gao L, Jiang Y, Ni R, Yang Q, Luo L (2021) A single-cell-resolution fate map of endoderm reveals demarcation of pancreatic progenitors by cell cycle. Proc Nat Acad Sci USA 118:e2025793118
56. Bakkers J (2011) Zebrafish as a model to study cardiac development and human cardiac disease. Cardiovasc Res 91:279–288
57. Tu S, Chi NC (2012) Zebrafish models in cardiac development and congenital heart birth defects. Differentiation 84:4–16
58. Staudt D, Stainier D (2012) Uncovering the molecular and cellular mechanisms of heart development using the zebrafish. Annu Rev Genet 46:397–418
59. He J, Lu H, Zou Q, Luo L (2014) Regeneration of liver after extreme hepatocyte loss occurs mainly via biliary transdifferentiation in zebrafish. Gastroenterology 146(789–800):e788
60. Liu C, Wu C, Yang Q, Gao J, Li L, Yang D, Luo L (2016) Macrophages mediate the repair of brain vascular rupture through direct physical adhesion and mechanical traction. Immunity 44:1162–1176
61. He J, Chen J, Wei X, Leng H, Mu H, Cai P, Luo L (2019) Mammalian target of rapamycin complex 1 signaling is required for the dedifferentiation from biliary cell to bipotential progenitor cell in zebrafish liver regeneration. Hepatology 70:2092–2106
62. Cai P, Mao X, Zhao J, Nie L, Jiang Y, Yang Q, Ni R, He J, Luo L (2021) Farnesoid X receptor is required for the redifferentiation of bipotential progenitor cells during biliary-mediated zebrafish liver regeneration. Hepatology 74:3345–3361
63. Chen J, He J, Ni R, Yang Q, Zhang Y, Luo L (2019) Cerebrovascular injuries induce lymphatic invasion into brain parenchyma to guide vascular regeneration in zebrafish. Dev Cell 49:697–710
64. Lombardo VA, Otten C, Abdelilah-Seyfried S (2015) Large-scale zebrafish embryonic heart dissection for transcriptional analysis. J Vis Exp 95:52087
65. Whelan JA, Russell NB, Whelan MA (2003) A method for the absolute quantification of cDNA using real-time PCR. J Immunol Methods 278:261–269